INS/GPS Fusion for Navigation of Unmanned Aerial Vehicles

Sanketh Ailneni[1], *Sudesh k. Kashyap*[2] *and Shantha Kumar N*[3]
[1, 2, 3] *National Aerospace Laboratories (CSIR-NAL), Bangalore, Karnataka, India*

This paper presents fusion of inertial navigation system (INS) and global positioning system (GPS) for estimating position, velocities, attitude and heading of an unmanned aerial vehicle (UAV). A 15 state extended Kalman filter (EKF) and a split architecture consisting of 6 state non-linear complementary filter (NCF) and 9 state EKF are investigated in detail. In both these fusion architectures GPS and IMU consisting of 3 axis accelerometers, 3 axis rate gyros and 3 axis magnetometer have been fused in open loop fashion (loosely coupled) to estimate the navigation states. These architectures have been implemented in MATLAB/SIMULINK environment and evaluated in closed loop guidance of MAV with Software-In-Loop-Simulation (SILS) setup. Furthermore, the 15-state EKF algorithm is validated with flight test data obtained from onboard data logger using an off-the shelf autopilot board (Ardupilot Mega APM-2.5) for UAV.

Nomenclature

INS	=	Inertial Navigation System
GPS	=	Global Positioning System
EKF	=	Extended Kalman Filter
NCF	=	Nonlinear Complementary Filter
SILS	=	Software in the Loop Simulations
MAV	=	Micro Aerial Vehicle
UAV	=	Unmanned Aerial Vehicle
MEMS	=	Micro Electro Mechanical Systems
DCM	=	Direction Cosine Matrix
AWGN	=	Additive White Gaussian Noise

I. Introduction

Micro-sized unmanned aerial vehicles (UAVs) or micro aerial vehicles (MAVs) require a high precision autonomous guidance navigation and control to carry out their missions successfully. This paper addresses navigation solution with INS/GPS fusion for MAVs. The INS/GPS fusion for flight vehicles is typically carried out through non-linear filtering approach which could be extended Kalman filter [EKF], unscented Kalman filters or non-linear complementary filters. MAVs make use of micro electro mechanical systems (MEMS) based inertial measurement unit (IMU) which comprise of tri-axial magnetometer to sense magnetic heading, tri-axial accelerometers to sense specific forces and a piezoelectric tri-axial gyros to sense the angular rates. These sensors are inherent to sensor noise, bias, scale factor and misalignment errors. As INS basically integrates the IMU data, the solution thus obtained will be drifting with time due to errors in inertial sensors. Fusion of IMU data and GPS measurements with the help of nonlinear filtering will improve the attitude and navigation solution.

The EKF based INS/GPS fusion approach is very well established for satellite and launch vehicle navigation using GPS carrier phase measurements [1]. Mahony.et.al. presented a novel NCF based attitude and heading deterministic observer [2], where in the kinematics are posed directly on the special orthogonal $SO(3)$ group driven by reconstructed attitude and angular velocity measurements . Venkatesh.et.al presented a novel

INS/GPS fusion architecture [3]. Quaternion representations of the attitude kinematics eliminate the singularity issues observed with Euler angle representation [4] [5].

This paper presents INS/GPS fusion for MAV with 15 state EKF and compared the performance with NCF-EKF split architecture based fusion algorithm. The performance of EKF based fusion approach is evaluated in the software in the loop simulation (SILS) setup for Black Kite MAV [14]. A comparative study was made with position, velocity, attitude and heading estimates from both the fusion architectures. Furthermore, the performance of 15-state EKF was evaluated with the flight test data of Sly-Bird UAV [14]. The flight test data was obtained from the autopilot board ARDU PILOT MEGA (APM – 2.5) with the help of onboard MEMS sensors and data logger. The position velocity and attitude estimates from the filter were compared with the reference DCM estimates from APM-2.5 [12].

This paper is structured as follows; Section II gives process and measurement mathematical models used in INS/GPS fusion architectures. Section III presents simulation scenario in the closed loop guidance (SILS) as well as the flight test scenario. Section IV presents the various simulation results and observations made. Section V presents the concluding remarks.

II. INS/GPS mathematical model formulation

The paper presents two INS/GPS fusion algorithms i) 15-state EKF ii) NCF-EKF Split architecture (6-state NCF + 9-state EKF) [3].

A. Sensor Model

The MEMS sensor suit consists of tri-axial accelerometers, tri-axial gyroscopes, tri-axial magnetometer and GPS.

Rate gyroscope:

The rate gyroscope measurements $p_m(t)$, $q_m(t)$, $r_m(t)$ are assumed to be modeled as:

$$\begin{aligned} p_m(\mathrm{t}) &= \mathrm{p}(t) + \left(b_{0_p} + \left(b_{1_p}(t) + b_{2_p}(t)\right)\right) + w_p \\ q_m(\mathrm{t}) &= q(t) + \left(b_{0_q} + \left(b_{1_q}(t) + b_{2_q}(t)\right)\right) + w_q \\ r_m(\mathrm{t}) &= r(t) + \left(b_{0_r} + \left(b_{1_r}(t) + b_{2_r}(t)\right)\right) + w_q \end{aligned} \qquad \textbf{Eq. 1}$$

where, $p(t)$, $q(t)$, $r(t)$ are the **true** values of the angular velocity; $b_{0p}(t)$, $b_{0q}(t)$, $b_{0r}(t)$ are the *constant null-shift* bias terms, $b_{1p}(t)$, $b_{1q}(t)$, $b_{1r}(t)$ are the *rate random walk* bias components, $b_{2p}(t)$, $b_{2q}(t)$, $b_{2r}(t)$ are the *correlated* (colored noise) bias components and w_p, w_q, w_r denote the error due to *sampling noise* which are typically modeled as zero mean, band-limited, additive, white Gaussian noise (AWGN) processes of specified covariances denoted by σ_p^2 , σ_q^2 , σ_r^2 respectively.

Note-1: *The constant bias components, b_{0p} , b_{0q} , b_{0r} , can be estimated off-line and removed from the output of the rate gyroscope. Hence, the effects of b_{0p} , b_{0q} , b_{0r} on the output of the rate gyroscope are neglected.*

Accelerometer:

The acclerometer measurements $a_{xm}(t)$, $a_{ym}(t)$, $r_{zm}(t)$ are assumed to be modeled as:

$$\begin{aligned} a_{x_m}(\mathrm{t}) &= a_x(t) + b_{a_x} + w_{a_x} \\ a_{y_m}(\mathrm{t}) &= a_y(t) + b_{a_y} + w_{a_y} \\ a_{z_m}(\mathrm{t}) &= a_z(t) + b_{a_z} + w_{a_z} \end{aligned} \qquad \textbf{Eq. 2}$$

where, b_{ax}, b_{ay} , b_{az} , are constant bias offsets, $a_x(t)$, $a_y(t)$, $a_z(t)$ are the **true** specific forces and w_{ax}, w_{ay} , w_{az} denote the additive sensor noise processes, respectively, for the *x, y, z* axes and are modeled as zero mean, band-limited AWGN processes with covariances denoted by $\sigma_{a_x}^2$, $\sigma_{a_y}^2$, $\sigma_{a_z}^2$ respectively.

GPS:

The GPS measurements *are* modeled as:

$$\begin{aligned} \lambda_m &= \lambda + v_\lambda & v_{n_m} &= v_n + v_{v_n} \\ \mu_m &= \mu + v_\mu & v_{e_m} &= v_e + v_{v_e} \\ h_m &= h + v_h & v_{d_m} &= v_d + v_{v_d} \end{aligned} \qquad \textbf{Eq. 3}$$

where, $v_\lambda, v_\mu, v_h, v_{v_n}, v_{v_e}, v_{v_d}$ denote zero mean, bandlimited, AWGN processes of covariances respectively denoted by σ_λ^2 , σ_μ^2 , $\sigma_h^2, \sigma_{v_n}^2$, $\sigma_{v_e}^2$, $\sigma_{v_d}^2$.

Note-2: *Thus from the sensor models one can notice that, the time varying bias in rate gyroscopes and constant bias in accelerometers have to be estimated online. Therefore these biases are included in the process model of the filters used in the state estimation.*

B. 15-state EKF

Neglecting the effect of Earth's rotation rate, the INS/GPS model in the local North-East-Down (NED) frame[1] is [9], [13]: with the notations

$$s_{\cdot} \equiv \sin(.); c_{\cdot} \equiv \cos(.); t_{\cdot} \equiv \tan(.)$$

$$\begin{bmatrix} \dot{\lambda} \\ \dot{\mu} \\ \dot{h} \end{bmatrix} = \underbrace{\begin{bmatrix} \dfrac{v_n}{R_M + h} \\ \dfrac{v_e}{(R_N + h)c_\lambda} \\ -v_d \end{bmatrix}}_{\begin{bmatrix} f_1 & f_2 & f_3 \end{bmatrix}^T} ;\sim\sim\sim \begin{bmatrix} \dot{v}_n \\ \dot{v}_e \\ \dot{v}_d \end{bmatrix} = \Re_B^I \begin{bmatrix} a_{x_m}(t) \\ a_{y_m}(t) \\ a_{z_m}(t) \end{bmatrix} + \underbrace{\begin{bmatrix} \dfrac{v_n v_d}{R_M + h} - \dfrac{v_e^2 t_\lambda}{R_N + h} \\ \dfrac{v_e (v_d + v_n t_\lambda)}{R_N + h} \\ \dfrac{-v_d^2}{R_M + h} - \dfrac{v_e^2}{R_N + h} + g \end{bmatrix}}_{\begin{bmatrix} f_4 & f_5 & f_6 \end{bmatrix}^T}$$

$$\begin{bmatrix} \dot{\psi} \\ \dot{\theta} \\ \dot{\phi} \end{bmatrix} = \underbrace{\begin{bmatrix} 0 & \dfrac{s_\phi}{c_\theta} & \dfrac{c_\phi}{c_\theta} \\ 0 & c_\phi & -s_\phi \\ 1 & s_\phi t_\theta & c_\phi t_\theta \end{bmatrix} \begin{bmatrix} p_m(t) \\ q_m(t) \\ r_m(t) \end{bmatrix}}_{\begin{bmatrix} f_7 & f_8 & f_9 \end{bmatrix}^T} ;\sim\sim\sim \begin{bmatrix} \dot{b}_{1_p} \\ \dot{b}_{1_q} \\ \dot{b}_{1_r} \end{bmatrix} = \begin{bmatrix} w_{1_p} \\ w_{1_q} \\ w_{1_r} \end{bmatrix} ;\sim\sim\sim \begin{bmatrix} \dot{b}_{a_x} \\ \dot{b}_{a_y} \\ \dot{b}_{a_z} \end{bmatrix} = \begin{bmatrix} w_{b_{a_x}} \\ w_{b_{a_y}} \\ w_{b_{a_z}} \end{bmatrix}$$

Eq. 4

where, λ, μ, h denote position (latitude, longitude and altitude), v_n, v_e, v_d denote velocities, ψ, θ, ϕ denote heading, pitch & roll, $w_{b_{a_x}}, w_{b_{a_y}}, w_{b_{a_z}}$ are zero mean, bandlimited, AWGN processes of specified covariances, R_M , R_N respectively denote the Earth's meridional and normal radius of curvature, $R_0 \approx 6378137m$, e = 0.081819190843 denote the Earth's radius and eccentricity respectively, g denotes the acceleration due to

[1] Locally, the North-East-Down frame is assumed to be inertial

gravity and $\Re_B^I = \left(\Re_I^B\right)^T$ is the rotation matrix that takes a vector from the body frame to the inertial frame. The expressions for R_M and R_N are given as:

$$R_M = R_0 \frac{\left(1-e^2\right)}{\left(1-e^2 s_\lambda^2\right)^{\frac{3}{2}}}; R_N = \frac{R_0}{\sqrt{\left(1-e^2 s_\lambda^2\right)}} \qquad \textbf{Eq. 5}$$

The EKF measurement model consists of GPS position, velocity and heading derived from a magnetometer and can be written as [10]:

$$\begin{aligned} \lambda_m &= \lambda + v_\lambda & v_{n_m} &= v_n + v_{v_n} \\ \mu_m &= \mu + v_\mu & v_{e_m} &= v_e + v_{v_e} \\ h_m &= h + v_h & v_{d_m} &= v_d + v_{v_d} \end{aligned} \qquad \textbf{Eq. 6}$$

$$\psi_m = \psi + v_\psi$$

where, $v_\lambda, v_\mu, v_h, v_{v_n}, v_{v_e}, v_{v_d}, v_\psi$ denote zero mean, bandlimited, AWGN processes of covariances respectively denoted by σ_λ^2, σ_μ^2, $\sigma_h^2, \sigma_{v_n}^2$, $\sigma_{v_e}^2$, $\sigma_{v_d}^2, \sigma_\psi^2$.

Note-3: *In this paper, the effects due to* b_{2_p}, b_{2_q}, b_{2_r} *are not captured in the model for the EKF, i.e.* b_{2_p}, b_{2_q}, b_{2_r} *are treated as* unmodeled *bias components, while the effects due to* b_{1_p}, b_{1_q}, b_{1_r} *are captured in the EKF model as Weiner process*[2] *components with however a different standard deviation for each of these components which alters the individual entries in the Q matrix.*

C. Split Architecture (6-state NCF + 9-state EKF)

As presented in [3], splitting the state vector in Eq. 4 such that (ψ, θ, ϕ), (b_{1_p}, b_{1_q}, b_{1_r}) are estimated via the 6 state NCF (AHRS formulation) while (λ, μ, h), (v_n, v_e, v_d) and ($b_{a_x}, b_{a_y}, b_{a_z}$) are estimated via 9 state EKF [10]. First the Euler angle estimates are obtained via the NCF solution and then fed into the EKF architecture to obtain the estimates of position and velocity. The NCF-EKF split architecture is shown in Fig. 1[3] where the KF block is the design of an EKF. The attitude kinematics is represented in direction cosine matrix (DCM) way and nonlinear complementary filter is directly implemented on SO(3) formed by DCM.

III. Simulation scenario

D. Software in the loop Simulation (Black Kite MAV)

A 6 DOF model complete with elevator and aileron control surfaces is used for the simulation study. The control loops are of proportional-integral-derivative type equipped with saturation and are similar to the control design suggested in [11], while velocity control is achieved via the throttle. Fig. 2 shows the software in the loop simulation (SILS) setup to evaluate and compare the performance of 15 state EKF and spilt architecture NCF-EKF in closed loop.

[2] A Wiener process is obtained by integrating the white noise process

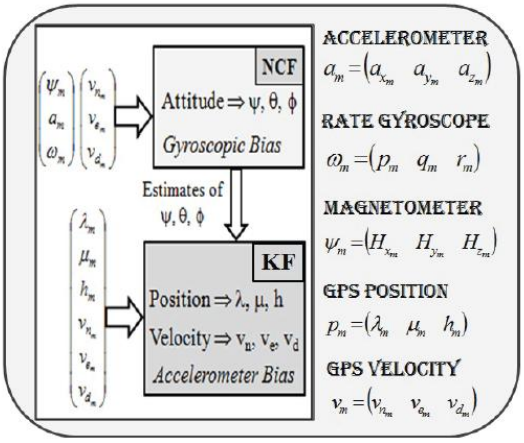

Fig. 1 Schematic view of Split architecture (NCF_EKF) [3]

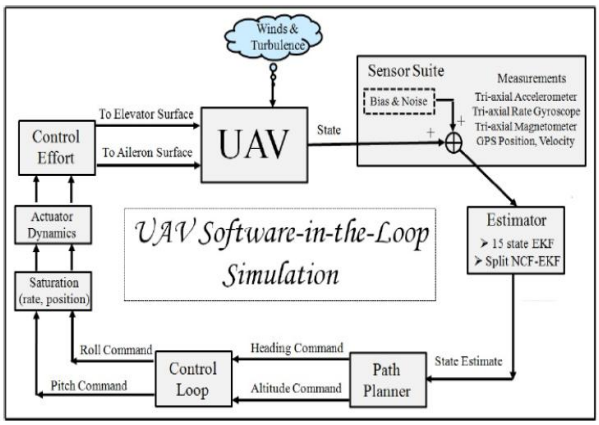

Fig. 2 Closed Loop simulations of a UAV with sensor and wind models

For simulation, the noise parameters are given as follows: $\sigma_p = \sigma_q = \sigma_r = 0.1\ ^\circ/s$, $\sigma_{1p} = \sigma_{1q} = \sigma_{1r} = 0.1\ ^\circ/s$, $\sigma_{2p} = \sigma_{2q} = \sigma_{2r} = 0.1^\circ/s$, $\sigma_{ax} = \sigma_{ay} = \sigma_{az} = 0.1\ m/s^2$, $\sigma_\psi = 0.5^\circ$. The time constant for the colored noise process is chosen as $\tau = 100$ s. The tri-axial accelerometer is assumed to have a constant bias of $b_{ax} = b_{ay} = b_{az} = 0.1m/s2$, while the tri-axial rate gyros is assumed to have a constant bias of $b_{0p} = b_{0q} = b_{0r} = 0.1^\circ/s$. The GPS noise parameters are given as $\sigma_\lambda = 6 \times 10{-}4\ deg$, $\sigma_\mu = 6 \times 10{-}5\ deg$, which approximately translates to 10 m error in the x and y axes, the standard deviation in the z axis is $\sigma_h = 10\ m$; the standard deviation in GPS velocities are $\sigma_{xgps} = \sigma_{ygps} = \sigma_{zgps} = 0.1m/s$. The update rate of the tri-axial accelerometers, rate gyros and magnetometers is 40 Hz and that of the GPS is 5 Hz. Thus the filter *prediction*, which requires accelerometers and rate gyros takes place at 40 Hz, while the measurement *corrections* with the magnetometer and the GPS occur at 40 and 5 Hz respectively.
The initial conditions for simulation model and the filter are:

$$\underbrace{x(0) = \begin{bmatrix} \lambda(0) \\ \mu(0) \\ h(0) \\ v_n(0) \\ v_e(0) \\ v_d(0) \\ \psi(0) \\ \theta(0) \\ \phi(0) \\ b_p(0) \\ b_q(0) \\ b_r(0) \\ b_{ax}(0) \\ b_{ay}(0) \\ b_{az}(0) \end{bmatrix} = \begin{bmatrix} 20^o \\ 70^o \\ 100m \\ 15m/s \\ 0 \\ 0 \\ 0 \\ 9^o \\ 0 \\ 0 \\ 0 \\ 0 \\ 0 \\ 0 \\ 0 \end{bmatrix}}_{Model} \quad \underbrace{\hat{x}(0) = \begin{bmatrix} \lambda(0) \\ \mu(0) \\ h(0) \\ v_n(0) \\ v_e(0) \\ v_d(0) \\ \psi(0) \\ \theta(0) \\ \phi(0) \\ b_p(0) \\ b_q(0) \\ b_r(0) \\ b_{ax}(0) \\ b_{ay}(0) \\ b_{az}(0) \end{bmatrix} = \begin{bmatrix} 0 \\ 0 \\ 0 \\ 0 \\ 0 \\ 0 \\ 0 \\ 0 \\ 0 \\ 0 \\ 0 \\ 0 \\ 0 \\ 0 \\ 0 \end{bmatrix}}_{Filter} \quad \textbf{Eq. 7}$$

The diagonal elements of 15-state EKF tuning parameter elements are:

$$Q_{ekf} = \left[10^{-2} I_3 \quad \left(\frac{0.005\pi}{180}\right)^2 I_6 \quad 10^{-4} I_3 \right]$$

$$P0_{ekf} = \left[\left(\frac{20\pi}{180}\right)^2 \quad \left(\frac{70\pi}{180}\right)^2 \quad 15^2 \quad 10^{-8} I_3 \quad \left(\frac{5\pi}{180}\right)^2 I_3 \quad \left(\frac{0.05\pi}{180}\right)^2 I_3 \quad 10^{-2} I_3 \right]$$

$$R_k = \left[\left(\frac{10^{-7}\pi}{180}\right)^2 \quad \left(\frac{10^{-7}\pi}{180}\right)^2 \quad 0.1^2 \quad 10^{-2} I_3 \quad \left(\frac{0.005\pi}{180}\right)^2 I_6 \right] \qquad \textbf{Eq. 8}$$

The NCF gains [3] for NCF-EKF split architecture are $k_P = 1$, $k_I = 0.1$.

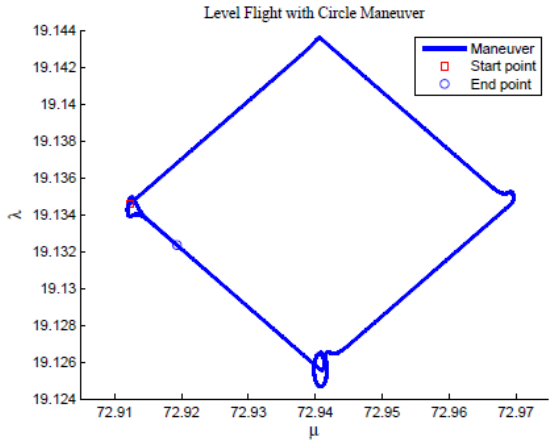

Fig. 3 Level Flight with Circle Maneuver

In the SILS environment both 15-state EKF and split architecture (NCF-EKF) are evaluated with the maneuver shown in the Fig. 3.

E. Performance of 15-state EKF with flight test data

The 15-state EKF was evaluated with the flight test data with the tuning parameters as given in Eq. 8.

The sensor suit in APM-2.5 board is listed below [12]:

Sensor suit on APM-2.5		
1)	Inertial Measurement Unit (IMU) a) 3-axis rate gyroscope b) 3-sxis accelerometers	Invensense MPU-6050
2)	3-axis magnetometer	HMC5843 sensor
3)	GPS	Ublox LEA-6H
4)	Pressure sensor	MS 5611
5)	Differential pressure sensor	Anlog device with Pitot probe

Table 1: Various sensors on APM-2.5

IV. Simulation Results & Discussion

F. SILS results with Black Kite MAV

The performance of the proposed filter architectures are carried out in closed loop simulation environment where the system dynamics and the senor dynamics are simulated with 6 DOF model of MAV (Black Kite). Simulations were carried out using the tuning parameters specified in the section III. Without changing the tuning parameters the robustness of the filter architectures is being studied. Fig. 4 and Fig. 5 show the performance of 15-state EKF and Split architecture NCF-EKF respectively. It is observed from Fig. 4(a), (b), (d), and Fig. 5(a), (b), (d) that the position, velocity and rate gyro bias state estimates are seen to track the true values in both the estimators. The error in attitude and heading estimates from Split architecture is higher than the estimates from 15 state EKF, reason being the assumption of negligible linear and lateral acceleration in the NCF formulation. And the accelerometer bias estimates in x and y directions using 15-state EKF and NCF-EKF split architecture is observed to be not as promising as we notice in the z direction which is seen in Fig. 4(e) and 5(e). Thus it is seen that the 15-state EKF and split architecture NCF-EKF state estimates are comparable for the manuver shown in Fig. 3. Both the filter architectures are further validated for various manuvers and the robustness of the algorithms are checked for various wind conditions.

G. Performance of 15 state EKF with flight test data

The 15 state EKF is further evaluated with the flight test data obtained from Sly-Bird UAV. APM-2.5 was integrated onboard and the logged sensor data for flight duration of 800 seconds was analysed. The EKF was implemented in open loop simulation environment and thus obtained estimates are compared against the APM-2.5 estimator (ARDU-DCM). Fig. 6 show the comparison between the EKF estimates with onboard ARDU-DCM estimates. It is observed that the EKF estimates are in comparison with the ARDU-DCM estimates. Fig. 6(d & e) show the estimates of gyro bias and accelerometer bias for flight trajectory with 800 seconds flight duration.

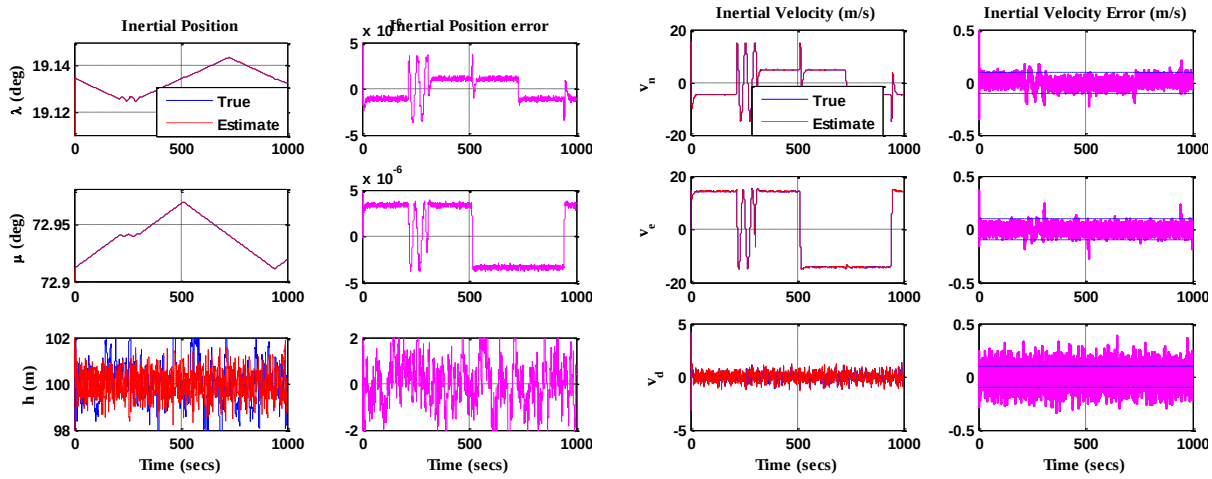

a. Position estimates

b. Velocity estimates

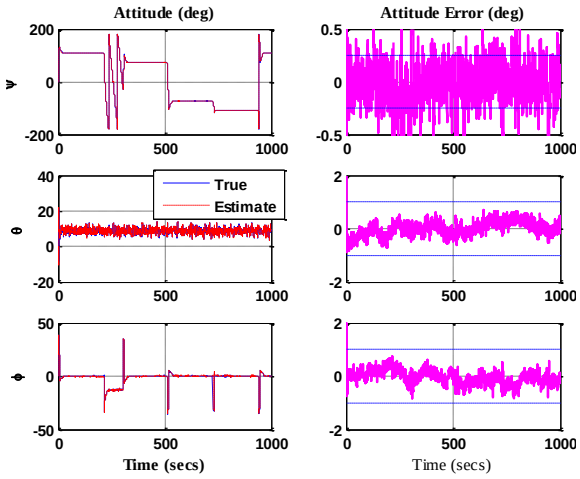

c. Attitude and heading estimates

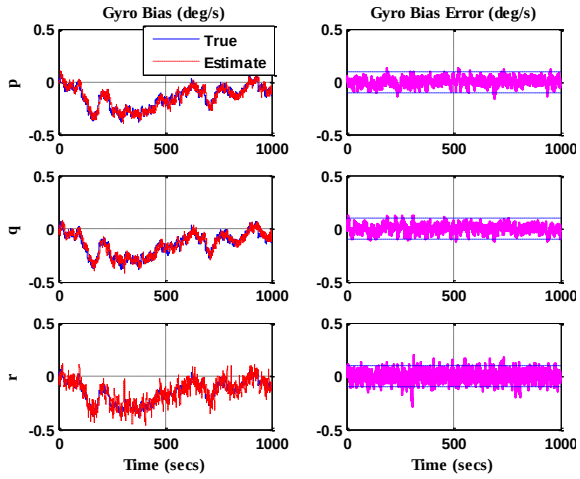

d. Gyro bias estimates

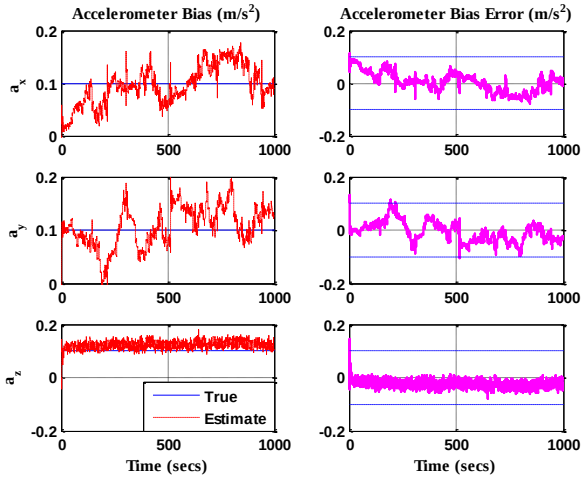

e. Accelerometer bias estimates

Fig. 4 Performance of 15-state EKF with the maneuver shown in Fig. 3

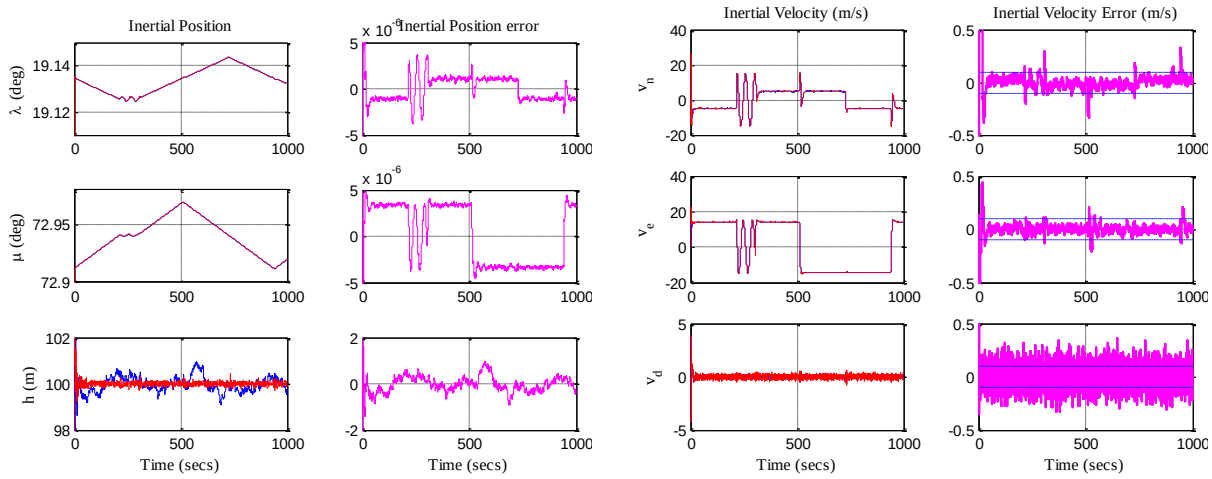

a. Position estimates

b. Velocity estimates

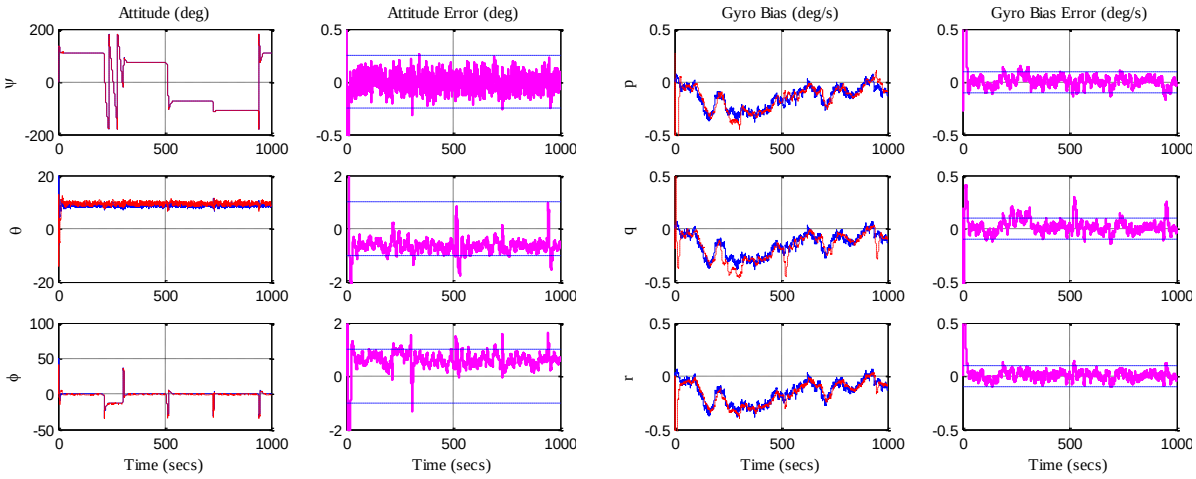

c. Attitude and heading estimates

d. Gyro bias estimates

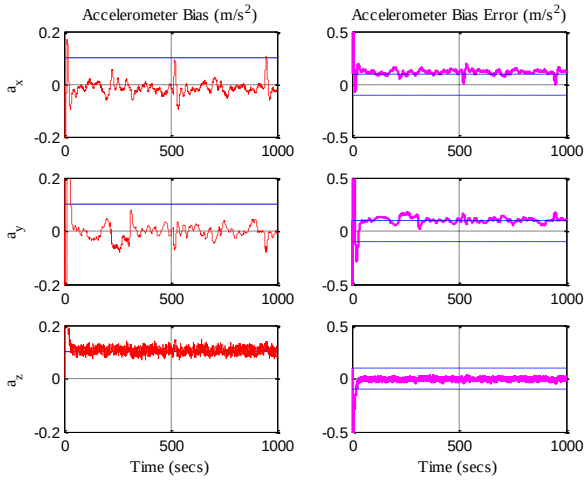

e. Accelerometer bias estimates

Fig. 5 Performance of NCF-EKF Split architecture with the manuver shown in Fig. 3

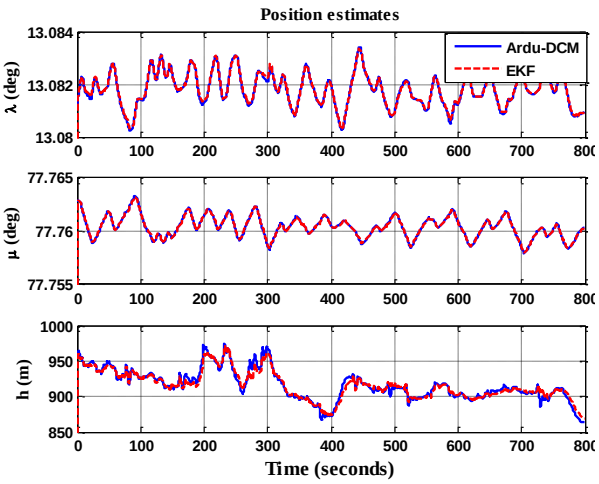

a. Position estimates

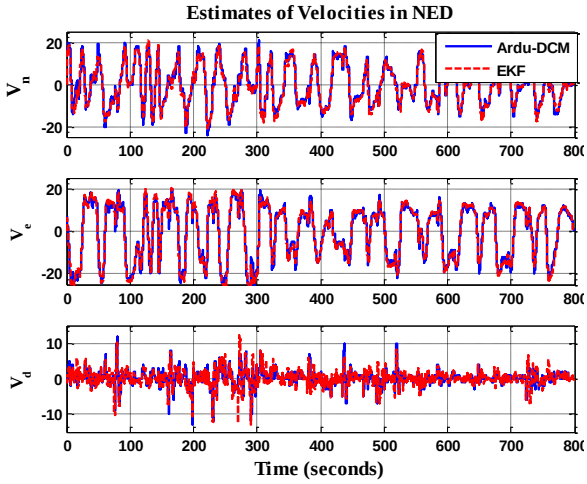

b. Velocity estimates

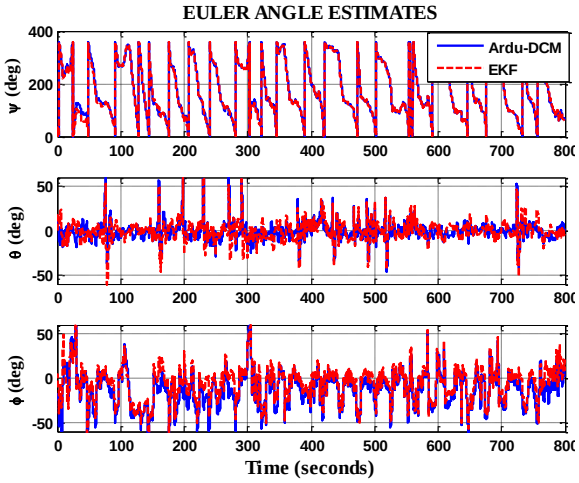

c. Attitude and heading estimates

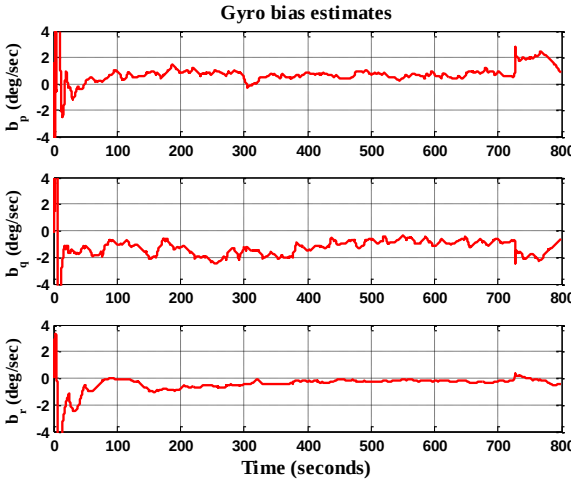

d. Gyro bias estimates

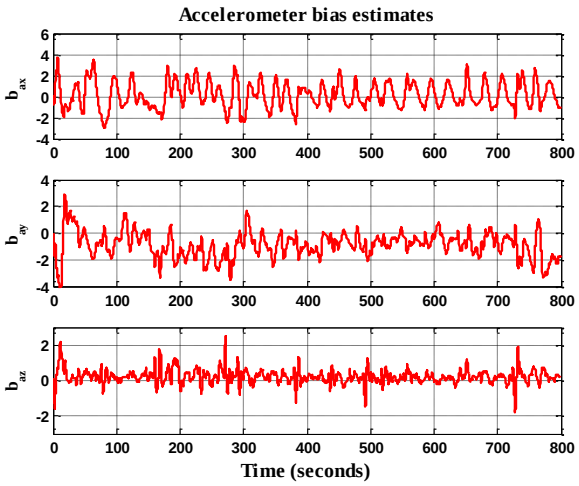

e. Accelerometer bias estimates

Fig. 6 Performance of 15 state EKF with the flight test data

V. Conclusion and Future work

Two INS/GPS fusion architectures namely 15 state EKF and NCF-EKF Split architecture for M/UAVs are investigated in SILS environment. It is observed that attitude and heading estimates are more accurate in the case of 15 state EKF compared to the NCF-EKF Split architecture, but attitude estimation via NCF in Split architecture is computationally less intensive compared to EKF architecture. It is also observed that the error in position, velocity and attitude estimates are well within the acceptable bounds for both the fusion architectures. Furthermore, the performance of 15 state EKF is evaluated with the flight test data obtained using Ardu Pilot Mega (APM-2.5) onboard Sly-Bird UAV. The position, velocities, attitude and heading estimates are observed to be in comparison with the onboard Ardu DCM estimator. Further research is in progress for evaluating both the estimators in hardware in the loop simulation (HILS).

Acknowledgments

NCF-EKF split architecture was originally developed by Venkatesh K Madyastha - Ex. Scientist of NAL. Authors express their sincere gratitude to the Flight test team at CSIR-NAL headed by Dr G.K Singh.

References

[1] James L. Farrell, "Carrier phase processing without integers", VIGIL *Inc*.
[2] R. Mahony, T. Hamel and J-M Pflimlin, "Nonlinear Complementary Filters on the Special Orthogonal Group", IEEE Transactions on Automatic Control, Vol. 53, No. 5, 2008, pp. 1203-1218.
[3] V. K. Madyastha, V. C. Ravindra and S. Mallikarjunan, "A Novel INS/GPS Fusion Architecture for Aircraft Navigation", 15*th* International Conference on information Fusion, Singapore, July 2012.
[4] S. Salcudean, "A globally convergent angular velocity observer for rigid body motion", IEEE Transactions on Automatic Control, Vol. 36, No. 12, 1991, pp. 1493-1497.
[5] J. Thienel and R. M. Sanner, "A coupled nonlinear spacecraft attitude controller and observer with an unknown constant gyro bias and gyro noise", IEEE Transactions on Automatic Control, Vol. 48, No. 11, 2003, pp. 2011-2015.
[6] F. Daum, "Nonlinear filters: beyond the Kalman filter", IEEE Aerospace and Electronic Systems Magazine, Vol. 20, No. 8, Aug. 2005, pp. 57 - 69.
[7] H. Nijmeijer and T. Fossen, New directions in nonlinear observer design, (Eds.) Lecture Notes in Control and Information Sciences 244, Springer Verlag, London, 1999
[8] R. Brown and P. Hwang, Introduction to Random Signals and Applied Kalman Filtering, John Wiley and Sons, Inc., 1992.
[9] D.H. Titterton and J.L. Weston, Strapdown Inertial Navigation Technology, IEE, 1997.
[10] Sanketh Ailneni, "Addressing issues in Inertial Navigation of Micro Aerial Vehicles(MAV) via an extended Kalman Filter with Biased Sensors", International Journal of Applied Research in Mechanical Engineering (IJARME), ISSN: 2231 –5950, Vol-2, Iss-2, 2012.
[11] Randal Beard, Derek Kingston, Morgan Quigley, Deryl Snyder, Reed Christiansen, Walt Johnson, Timothy McLain and Michael A. Goodrich, "Autonomous Vehicle Technologies for Small Fixed-Wing UAVs", Journal Of Aerospace Computing, Information, And Communication Vol.2, January 2005.
[12] DIY Drones open source official repository for Ardupilotmega 2.5. "https://code.google.com/p/ardupilot-mega/wiki/APM25board".
[13] Sanketh Ailneni, "Multi rate sensors based inertial navigation for micro aerial vehicles," M-Tech. Dissertation, Flight Mechanics and Controls Division (CSIR-NAL), AcSIR Univ., Bangalore, Aug, 2012.
[14] CSIR – National Aerospace Laboratories, MAV design group. "http://www.nal.res.in/pages-/developmentofMav.htm".